J Nanopart Res (2013) 15:1436
DOI 10.1007/s11051-013-1436-5

RESEARCH PAPER

A luminescent supramolecular assembly composed of a single-walled carbon nanotube and a molecular magnet precursor

G. A. M. Sáfar · T. R. G. Simões · A. M. de Paula · X. Gratens · V. A. Chitta · H. O. Stumpf

Received: 20 August 2012 / Accepted: 11 January 2013 / Published online: 24 January 2013

Abstract Magnetism of supramolecular assemblies of single-walled carbon nanotubes (SWCNTS) with a magnetic dinuclear molecule is investigated. Raman, optical absorption and confocal fluorescence images are used to probe the interaction of the dinuclear compound and the SWCNT. The supramolecular assembly shows antiferromagnetism, on the contrary to the case when strong electronic doping of the SWCNT occurs, yielding a spin-glass system, and contrary to the case of the dinuclear molecular crystal, which is ferromagnetic. The SWCNT imposes the antiferromagnetic order to the dinuclear molecule, corroborating recent findings that antiferromagnetism is present in pure SWCNTs. Two theoretical models are used to fit the data, both yielding good fitting results. The nanoparticle size range is around 2–10 nm.

G. A. M. Sáfar (✉) · T. R. G. Simões · H. O. Stumpf
Departamento de Química, Universidade Federal de Minas Gerais, Belo Horizonte, MG 31270-901, Brazil
e-mail: gamsafar@yahoo.com.br

A. M. de Paula
Departamento de Física, Universidade Federal de Minas Gerais, Belo Horizonte, MG 31270-901, Brazil

X. Gratens · V. A. Chitta
Instituto de Física, Universidade de São Paulo, São Paulo, SP, Brazil

Keywords Magnetic properties · Single-walled carbon nanotubes · Antiferromagnetic · Mean field theory · Magneto-anisotropic nanoparticles

Introduction

Antiferromagnetism in single-walled carbon nanotubes (SWCNTs) has been overlooked since its discovery (Islam et al. 2005). Nonetheless, recently the subject has attracted considerable attention (Likodimos et al. 2007; Sáfar et al. 2012). Antiferromagnetism is important in SWCNT due to the relation of the electronic structure of SWCNT to its magnetic properties. The zigzag border of SWCNT is responsible both for the origin of the semiconductor or the semi-metallic character trend of SWCNT (Hamada et al. 1992; Mintmire et al. 1992; Saito et al. 1992) and for the origin of antiferromagnetism (Kim et al. 2003; Sáfar et al. 2012). Then, in principle, the antiferromagnetism is present in almost every allotropic form of carbon, the only exception being the fullerenes and the armchair nanotubes. Thus, for the design of a spintronic circuit based on SWCNT, one must concern about the chiral index of each SWCNT that composes the circuit.

Also, studies of supramolecular assemblies of molecular magnets and SWCNTs have drawn considerable attention because of the possibilities of applications on spintronic devices (Dul et al. 2010;

Ferrando-Soria et al. 2012). Nonetheless, the preparation of such assemblies is not straightforward, especially when the molecules are synthesized directly on the SWCNT surface (Chichak et al. 2005; Steuerman et al. 2002).

First, the adsorption of the molecule onto the SWCNT must be obtained and studied. It is interesting to choose a luminescent molecule to be adsorbed onto the SWCNT in order to be able to study the adsorption by luminescence. In some cases, luminescent molecules adsorbed on or covalently linked to SWCNT can still show luminescence (Lu et al. 2009; Qian et al. 2011; Wang et al. 2010). However, luminescence quenching can sometimes happen due to different phenomena like charge transfer or Forster effect (Tan et al. 2007).

Raman spectroscopy can also be used to investigate the adsorption. However, due to the large Raman cross section of SWCNT (Bohn et al. 2010) the observed Raman signal is mainly due to the Raman scattering coming from the SWCNT. But it was demonstrated that without net charge transfer between the molecule and the SWCNT, the main observed features of a SWCNT Raman spectrum do not change (Park et al. 2009).

In this work, we report a study of a supramolecular assembly of SWCNT and a metallocyclophane (Du et al. 2006; Dul et al. 2010; Fernandez et al. 2001; Ferrando-Soria et al. 2012; Hua and Lin 2004; Lin et al. 2004; Pardo et al. 2009; Pereira et al. 2004), $Na_4[Cu_2(mpba)_2]\cdot 8H_2O$ [mpba = *meta*-phenylenebis(oxamato)]. The green-yellow luminescence of $Na_4[Cu_2(mpba)_2]\cdot 8H_2O$ can be used to track the molecule in the assembly $Na_4[Cu_2(mpba)_2]\cdot 8H_2O$/SWCNT. Results of fluorescence, Raman spectroscopy, optical absorption and magnetic measurements are presented. We demonstrated that, differently from previous studies, the supramolecular assembly shows negligible charge transfer between its components (Sáfar et al. 2012). This feature modifies the overall magnetic behavior.

Experimental

$Na_4[Cu_2(mpba)_2]\cdot 8H_2O$ was synthesized following a method already described in the literature (Fernandez et al. 2001). Magnetic measurements of the pure substance were kindly provided by Prof. Miguel Julve Olcina (data not shown). The measurements show the same results as in the work of Fernandez et al. (2001).

A volume of 25 mL of an aqueous solution containing 0.80 g of NaOH (20.0 mmol) is added to a suspension containing 1.54 g (5.0 mmol) of mpba = *meta*-phenylenebis(oxamato) in 250 mL of water at 60 °C. The mixture was allowed to react, at 60 °C, for 20 min, with constant agitation. After cooling down to room temperature, 50 mL of an aqueous solution containing 1.20 g (5.0 mmol) of $Cu(NO_3)_2\cdot 3H_2O$ was added, drop by drop, slowly and with constant stirring. Subsequently, it was centrifuged and the solid was removed. After, the volume of the solution was reduced to almost complete dryness. The obtained solid was washed with ethanol and subsequently with ether. The resulting green powder was dried under vacuum. The yield was 69 % (1.49 g, 1.73 mmol).

CoMoCAT (Cobalt Molybdenum Catalysts) SWCNT sample was purchased from SWeNT® (South Western Nanotechnologies) and used without further purification. Electron paramagnetic resonance spectra measured in the raw SWCNT sample showed no signal at room temperature and transmission electron microscopies showed very low catalyst content (data not shown). The full characterization of the pristine SWCNT sample is reported elsewhere, showing that the catalysts nanoparticles have no influence in the overall magnetic signal (Sáfar et al. 2012).

A quantity of 2.00 mg of $Na_4[Cu_2(mpba)_2]\cdot 8H_2O$ and 0.80 mg of CoMoCAT were added to 10 mL of H_2O and sonicated at high power for 30 min. Another quantity of 0.80 mg of CoMoCAT was added to 10 mL of H_2O and 200.00 mg of sodium dodecylsulfate (SDS), solely to serve as a blank for the optical absorption spectra. Following preparation, the optical properties of the non-covalently functionalized SWCNT with $Na_4[Cu_2(mpba)_2]\cdot 8H_2O$, i.e., the supramolecular assembly were studied by absorption, photoluminescence, and Raman spectroscopy.

The optical absorption measurements were performed using a Hitachi U-2010 spectrophotometer on the suspensions/solutions. The photoluminescence (PL) were obtained in the solution and in the dried sample. The multiphoton PL of the solution in a quartz cuvette were measured with excitation by two photons at 800 nm from a femtosecond pulsed Ti–sapphire laser (Chameleon Coherent) and an Andor spectrometer coupled to a CCD detector. Images of the PL on a dried grain were obtained using an Olympus FV300 confocal system in an up-right configuration (BX61WI microscope) with a 60X objective and

excitation by an argon laser at the wavelength 488 nm. The images were collected in the wavelength range 510–600 nm. Raman spectra were recorded using a T64000 micro-Raman spectrometer operating with an excitation wavelength of 647 nm. Magnetic measurements were performed using a superconducting quantum interference device magnetometer.

Experimental results and discussion

Figure 1 shows the fluorescence spectra of the $Na_4[Cu_2(mpba)_2]\cdot 8H_2O$/SWCNT supramolecular assembly in water suspension. The peak observed at 550 nm is originated by the $Na_4[Cu_2(mpba)_2]\cdot 8H_2O$ molecule. Figure 2 shows the optical absorption spectra of the $Na_4[Cu_2(mpba)_2]\cdot 8H_2O$/SWCNT, SWCNT/SDS, and the $Na_4[Cu_2(mpba)_2]\cdot 8H_2O$ (in water). Most probably, the electronic transition that represents the emission at 550 nm is generated by absorption of two 800 nm photons, that means an excitation at 400 nm, where there is a strong absorption peak (Fig. 2). The presence of fluorescence indicates that quenching is a minor effect, if there is any.

We had made ordinary spectrofluorimetry in the samples, also in water solution, to avoid black-body radiation build up (Fainchtein et al. 2012). The signal was pretty much the same. However, the intensity of the signal was poor, with a high noise/signal ratio.

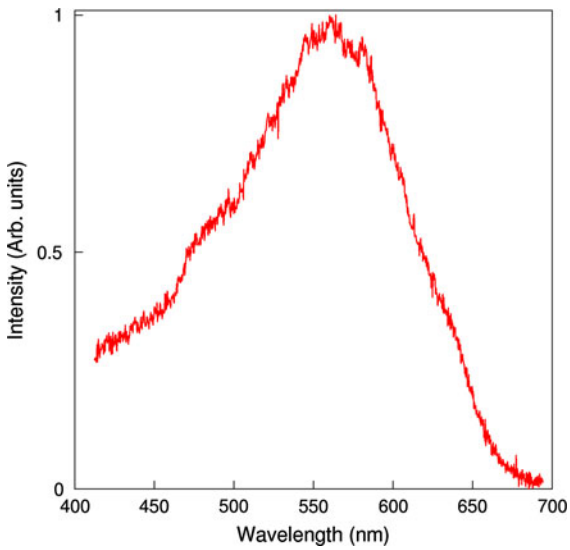

Fig. 1 Fluorescence spectra for $Na_4[Cu_2(mpba)_2]\cdot 8H_2O$/SWCNT

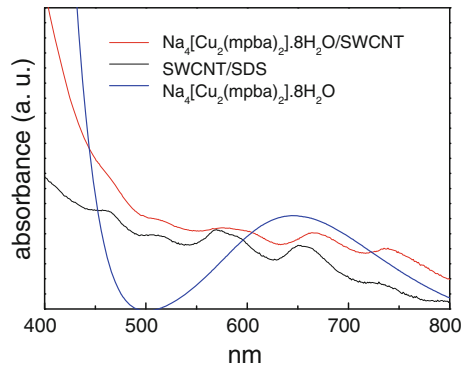

Fig. 2 Optical absorption spectra of SWCNT/SDS and $Na_4[Cu_2(mpba)_2]\cdot 8H_2O$/SWCNT, and $Na_4[Cu_2(mpba)_2]\cdot 8H_2O$

Researchers have reported defect induced luminescence from pristine SWNTs (Gupta et al. 2011). However, we had no sign of luminescence in the pristine SWCNT samples in the investigated spectral range that we have used. That is no surprise, since different growth methods can yield different nanotube chiral indexes.

A series of confocal fluorescence microscopies was made with an excitation at 488 nm (collected with a filter of 530−560 nm). Fluorescence appears to be originated mostly from the SWCNT agglomerates as can be seen in Fig. 3.

Raman spectra of the same $Na_4[Cu_2(mpba)_2]\cdot 8H_2O$/SWCNT sample can be compared to the pure SWCNT spectra in Fig. 4a for the radial breathing mode (RBM) region and in Fig. 4b for the G band region. The spectra of all the organic compounds used in this work have no features in the RBM region ($\lambda = 647$ nm). Therefore, all the peaks observed in Fig. 4a are due to SWCNT and $Na_4[Cu_2(mpba)_2]\cdot 8H_2O$/SWCNT. Due to the large Raman cross section of SWCNT (Bohn et al. 2010), peaks from $Na_4[Cu_2(mpba)_2]\cdot 8H_2O$ are not observed in Fig. 4. For both bands, we observe a frequency shift of the $Na_4[Cu_2(mpba)_2]\cdot 8H_2O$/SWCNT spectra relative to the SWCNT spectra. This shift is more clearly observed in Fig. 4b.

In the synthesis of the $Na_4[Cu_2(mpba)_2]\cdot 8H_2O$/SWCNT, no extra surfactant was used. The reason is that $Na_4[Cu_2(mpba)_2]\cdot 8H_2O$ is a surfactant for SWCNT. In other words, $Na_4[Cu_2(mpba)_2]\cdot 8H_2O$ is in close contact with the SWCNT. This and the observation of a frequency shift in the Raman spectra indicate the existence of a charge transfer from

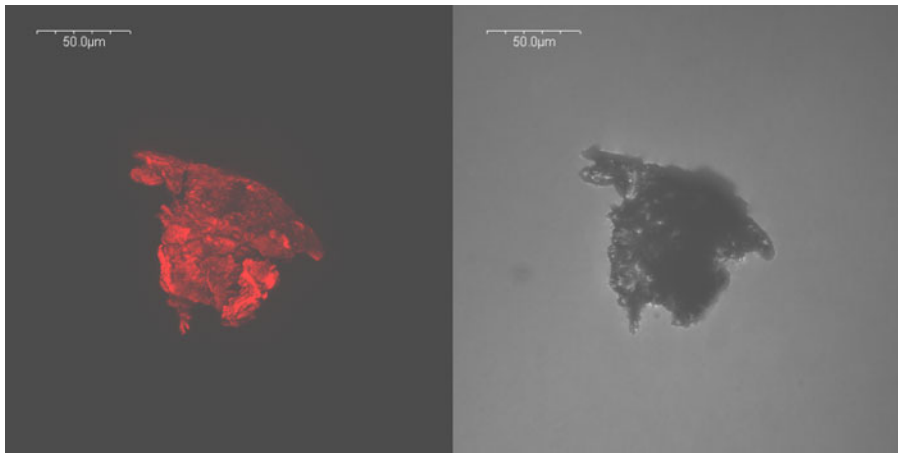

Fig. 3 Confocal fluorescence images (*right*: fluorescence; *left*: transmitted light). Both pictures, obtained simultaneously, show the same region on a microscope glass slide. Most of the collected light at 530−560 nm (artificially colored *red*) comes from the SWCNT agglomerates (*dark* grains). (Color figure online)

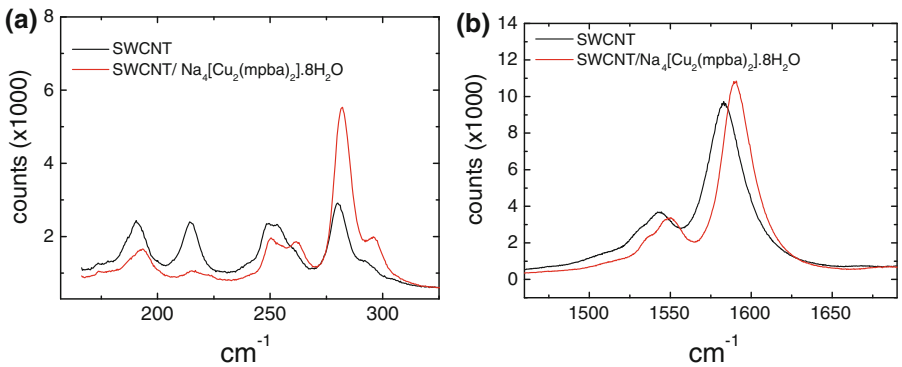

Fig. 4 Raman spectra of SWCNT and $Na_4[Cu_2(mpba)_2]\cdot 8H_2O$/SWCNT: **a** RBM region and **b** G band region (excitation at $\lambda = 647$ nm)

$Na_4[Cu_2(mpba)_2]\cdot 8H_2O$ to SWCNT. This charge transfer is relatively weak because it gives rise to a small shift of the peaks of the G band (~ 10 cm^{-1}). Raman energy shifts and surfactation show that $Na_4[Cu_2(mpba)_2]\cdot 8H_2O$/SWCNT forms a homogeneous system. Another indication of that is the increase of amplitude of the peak near 282 cm^{-1} for the $Na_4[Cu_2(mpba)_2]\cdot 8H_2O$/SWCNT in comparison to the SWCNT spectra. We suggest that this happens because $Na_4[Cu_2(mpba)_2]\cdot 8H_2O$ has an absorption peak at the laser excitation of 647 nm (see Fig. 2), giving rise to a Raman resonance. This could also suggest that there is a selective adsorption of the $Na_4[Cu_2(mpba)_2]\cdot 8H_2O$ on small-diameter SWCNT (Sáfar et al. 2010).

Figure 5 shows the zero-field cooled (ZFC) and field cooled (FC) magnetization measured as a function of the temperature and for different values of the magnetic field for the $Na_4[Cu_2(mpba)_2]\cdot 8H_2O$/SWCNT sample. Comparison of the present results with previous works on SWCNT and on the supramolecular assembly of SWCNT and metalloporphyrin corroborates the following overall picture (Sáfar et al. 2012). Whenever there is a significant charge transfer between the magnetic adsorbate and the SWCNT, the original SWCNT antiferromagnetic system (pure SWCNT in a superparamagnetic form) can change to a spin-glass system (Sáfar et al. 2012). In such case, the bifurcation temperature in ZFC–FC curves follows the de Almeida–Thouless (AT) line (Almeida and

Thouless 1978), where $\delta T_F \sim H^{2/3}$. This is not the case for the $Na_4[Cu_2(mpba)_2]\cdot 8H_2O$/SWCNT, where the charge transfer is not strong enough to disturb the antiferromagnetic ordering, thus the resulting superparamagnetism has apparently a blocking temperature of 300 K, as already stated for pure SWCNT (Islam et al. 2005). Figure 5 clearly shows that the separation between the ZFC and the FC curves obtained for the same magnetic field value occurs at 300 K. This feature is observed for all values of the magnetic field. However, when compared to a system where doping takes place, the system shows a magnetization even lower in the high temperature range with low applied field (Sáfar et al. 2012). Most probably, this is because of the reinforcing magnetic order of the SWCNT, which is antiferromagnetic, that is imposed to the magnetic adsorbate. Purely antiferromagnetic systems have the same blocking temperature as the applied field is increased. Here, we have no shift of the blocking temperature, indicating a purely antiferromagnetic system in both pristine SWCNT and $Na_4[Cu_2(mpba)_2]\cdot 8H_2O$/SWCNT cases.

The saturation magnetization per mass of the pure SWCNT (1.5 emu/g) is lower than that of the $Na_4[Cu_2(mpba)_2]\cdot 8H_2O$/SWCNT system (3 emu/g), which is also lower than that of the pure $Na_4[Cu_2(mpba)_2]\cdot 8H_2O$ (12.5 emu/g). A weighted average for the pure substances would give 9.3 emu/g. Moreover, the pure $Na_4[Cu_2(mpba)_2]\cdot 8H_2O$ is ferromagnetic (Fernandez et al. 2001). Therefore, the spins from the Cu atoms in the $Na_4[Cu_2(mpba)_2]\cdot 8H_2O$ molecule are reorganized by the spins originated from the SWCNT, forming a more stable antiferromagnetic arrangement, when in an external magnetic field, than that of the pure SWCNT ordering. The higher value of the magnetization saturation in low temperature also indicates that, contrary to the doping case (Sáfar et al. 2012), new spins are added to the system corresponding to the added magnetic atoms as already expected.

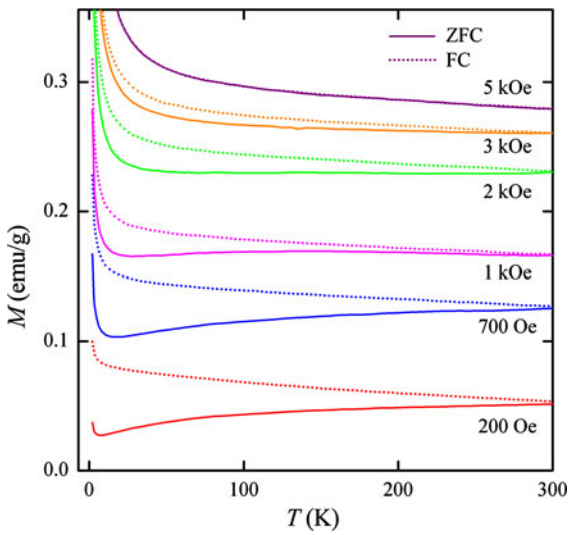

Fig. 5 ZFC−FC curves of the magnetization as a function of the temperature for the $Na_4[Cu_2(mpba)_2]\cdot 8H_2O$/SWCNT sample. The solid lines represent the ZFC data. The *dotted lines* represent the FC results. The figure clearly shows that the separation between the ZFC and the FC curves obtained for the same magnetic field value occurs at 300 K. This feature is observed for all values of the magnetic field

As in the case of a magnetic adsorbate, which is also an electronic dopant, the $Na_4[Cu_2(mpba)_2]\cdot 8H_2O$ diminishes the magnetization of the SWCNT system, at low magnetic field and high temperature. In this way, the argument used in a previous work to assure that the SWCNT samples were particularly pure, in respect to nanoparticle contamination, is now not necessary (Sáfar et al. 2012). For instance, if any nanoparticle was involved in the magnetic signal generation, the variation in the saturation magnetization (Ms) would behave like in a system investigated by Gupta et al. (2011) where Ni nanoparticles are profuse in the SWCNT sample and the Ms varies very little with the increasing temperature, up to 300 K. In the work of Gupta, the magnetization–temperature curve depicts a typical ferromagnetic like curve with a Curie temperature of 400 °C (Gupta et al. 2011). This is not the case here, where the Ms falls rapidly with increasing temperature, reaching a quasi-plateau already at 200 K (see trend of 5 kOe curve, Fig. 5).

When the $Na_4[Cu_2(mpba)_2]\cdot 8H_2O$ is adsorbed on the SWCNT, the magnetization is around 4–5 times lower than the magnetization of pristine SWCNT in low field (200 Oe), and 2 (2 K) to 4 (300 K) times in high field (3 kOe) when compared, again, to the pure SWCNT magnetization. That would not happen if the antiferromagnetism was coming from any metallic contamination (catalyst nanoparticles) in the sample. Moreover, neither a hyperbolic tangent nor a Langevin function can fit the M versus H hysteresis loop curves, measured at $T = 30$ K and $T = 3$ K for the $Na_4[Cu_2(mpba)_2]\cdot 8H_2O$/SWCNT sample, shown in Fig. 6. That means that ideal superparamagnetism fails to describe these systems.

The magnetism observed in the samples cannot be explained by the Co/CoO of the catalyst nanoparticles. First, the FC–ZFC magnetization curves in Fig. 5 are not typical curves of Co/CoO nanoparticles (with average radius varying from 3 to 20 nm depending on the synthetic route) (Das et al. 2009; Feygenson et al. 2010; Gonzalez et al. 2009; Shina et al. 2010). Moreover, although CoO shell is antiferromagnetic, Co/CoO nanoparticles show ferromagnetic behavior (ZFC curve) (Das et al. 2009; Feygenson et al. 2010; Gonzalez et al. 2009; Shina et al. 2010).

To better understand the magnetic structure of the system at low temperature, we have analyzed the magnetization traces using two models. One model is the magneto-anisotropic nanoparticle model (MANAM) (Bandyopadhyay 2009), in which a collection of non-interacting three-dimensional (3D) magnetically anisotropic nanoparticles is considered. In that model, the ratio between the magnetization of a nanoparticle which obeys the Langevin function and one which obeys the Ising model is roughly an exponential function of the applied field (Bandyopadhyay 2009). In our system, there are various possible positions where the $Na_4[Cu_2(mpba)_2]\cdot 8H_2O$ molecule can adsorb onto the SWCNT. At each position the molecule has a different anisotropy constant, which gives a different anisotropy constant to each particular molecule.

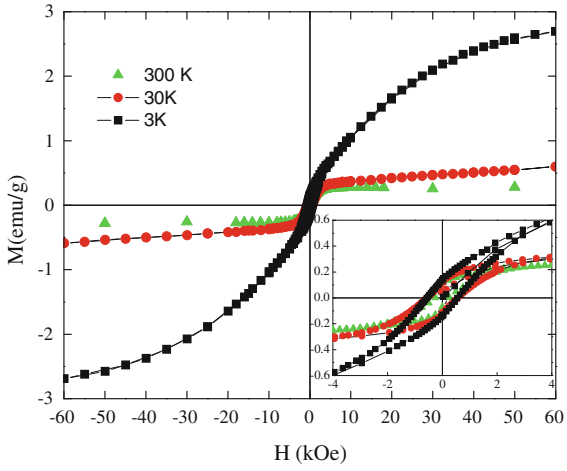

Fig. 6 M versus H hysteresis loops for a $Na_4[Cu_2(mpba)_2]\cdot 8H_2O$/SWCNT sample. The *inset* shows the low field part around the origin of the hysteresis loops. No diamagnetic correction was made

In a second model, we have considered the mean field theory approximation (MFT) (Li and Greaves 2004). Again, the random distribution of the $Na_4[Cu_2(mpba)_2]\cdot 8H_2O$ molecules causes an average field, or mean field, of each molecule on the nearest molecule adsorbed on the SWCNT and on the delocalized electrons of the SWCNT and vice versa. There are two sub-lattices of spins, one from $Na_4[Cu_2(mpba)_2]\cdot 8H_2O$ molecule with $S = 1$ and the second from the nanotube with $S = ½$. Both sub-lattices experiment the same effective field H_{eff}.

In our case, we were able to fit the magnetization dependence on the applied field by the following expression (MFT model)

$$M = M_0 \frac{e^h - e^{-h}}{e^d + e^h + e^{-h}} + M_1 \tanh\left(\frac{h}{2}\right) \qquad (1)$$

where M is the magnetization, $d{=}D/kT, h = g\mu_B H_{\text{eff}}/KT$, $H_{\text{eff}} = H_0 + \lambda M$, and $\lambda = 2zJ/Ng^2B^2$.

For the MANAM model, we also assume two sub-lattices of spins, also with different populations. Since magnetization is an intensive variable, we used a normalized curve obtained from one of our references (Bandyopadhyay 2009). For both models, $M_s = M_0 + M_1$. The results of the fit of the magnetization trace measured at $T = 3$ K are displayed in Fig. 7.

Using the linear chain model, the fitting procedure gives $\langle\lambda\rangle = 0.37(3)$, $\langle g\rangle = 2.490(6)$, and $\langle D\rangle \cong 0$. We believe that these values are average values because of the random positions of the molecules adsorbed on the SWCNT. The vanishingly small value of D is not surprising, as the delocalized electrons of SWCNT can shield more effectively both electric and magnetic fields, yielding, in average, an isotropic molecular field. This could also be the reason for the high value of $\langle\lambda\rangle$.

We obtained good fits of the magnetization trace with both models. This can be due to the similarities between the models: a linear chain of interacting spins, with a nearest-neighbor correlation length, that can be viewed as a collection of non-interacting three-dimensional (3D) magnetically anisotropic nanoparticles, with an occasional gap in the chain. Figure 8 shows a schematic view of how the models are similar.

The mean field linear chain model better fits the data than the Ising model of non-interacting three-dimensional magnetically anisotropic nanoparticles. However, the latter seems to be a good approximation.

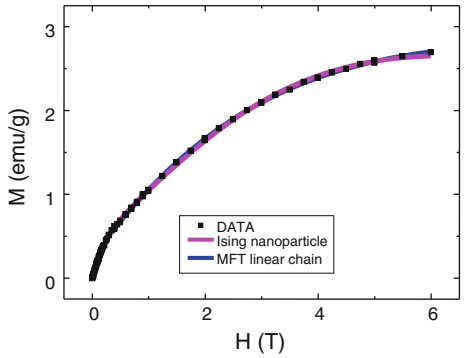

Fig. 7 First Magnetization trace of $Na_4[Cu_2(mpba)_2]\cdot 8H_2O$/SWCNT at $T = 3$ K. The MFT model curve of a linear chain and the MANAM model curve are shown

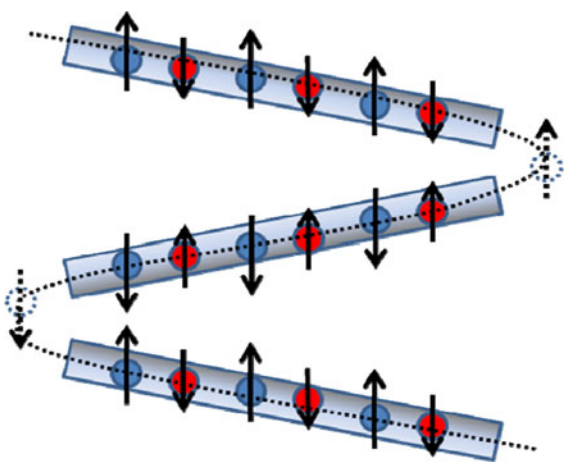

Fig. 8 A collection of non-interacting three-dimensional (3D) magnetically anisotropic nanoparticles as a 1-dimensional chain, with an occasional "gap" in the chain. The schematic view is highly idealized, but the representation can approach the mean field theory by averaging distances, molecular positions, etc

At a first look, the agreement of both models to the curve is a coincidence.

Both models have four fitting parameters, not considering the D parameter ($D = 0$). We choose not to add any other parameter to avoid overfitting. However, to fit M versus H at $T = 30$ K, a Langevin function is better. One possible reason for the difference between the M versus H hysteresis loops, at $T = 3$ K (MFT or MANAM) and $T = 30$ K (Langevin), is because the value of g for a nanotube is a function of the temperature (Beuneu et al. 1999). That was observed for multi-walled carbon nanotubes, although here the principle is the same: the delocalized electrons have a free-electron g value and the defects have a different g value (Beuneu et al. 1999). In our case, the $Na_4[Cu_2(mpba)_2]\cdot 8H_2O$ molecules can be viewed as defects, especially because a net diamagnetism, present in pure SWCNT samples, is destroyed when the $Na_4[Cu_2(mpba)_2]\cdot 8H_2O$ adsorbs onto the SWCNT. This was already observed in porphyrin doped SWCNT (Sáfar et al. 2012).

However, the analytical expression for g(T), (found in Beuneu et al. 1999), is not useful in our case, because there are possibly two processes occurring here. One is caused by the nanostructured size of the system and related to the blocking temperature at $T = 300$ K (Islam et al. 2005). The other is a phase transition or, most probably, a quasi-phase transition under 5 K which is related to the two sub-lattices composed by paramagnetic centers of the $Na_4[Cu_2(mpba)_2]\cdot 8H_2O$ and the SWCNT. We believe that is the case because, as mentioned above, there is a difference between the hysteresis loops at $T = 3$ K and $T = 30$ K. Moreover, the temperature dependence observed in Fig. 5 shows an abrupt change of magnetization at 5 K, which is related to the two sub-lattices composed by paramagnetic centers of the $Na_4[Cu_2(mpba)_2]\cdot 8H_2O$ and the SWCNT. We can say that $Na_4[Cu_2(mpba)_2]\cdot 8H_2O$ and SWCNT are interacting magnetically because the susceptibility of $Na_4[Cu_2(mpba)_2]\cdot 8H_2O$/SWCNT is lower than that of pure SWCNT (Sáfar et al. 2012) (and pure $Na_4[Cu_2(mpba)_2]\cdot 8H_2O$) (Fernandez et al. 2001) from 2 to 300 K, up to $H = 5$ kOe. In any case, further studies are necessary to better understand the system, mainly in what concerns the temperature dependent magnetization.

Finally, similarities between doped and undoped systems are the absence of a net diamagnetism, compared to the pure SWCNT case. That is due to the stronger localization caused by the perturbation in the nanotube Hamiltonian, which comes from the adsorbed magnetic molecules and the lower magnetization at high temperature.

Conclusions

In conclusion, the magnetism of molecular magnets/SWCNT supramolecular assemblies can differ drastically from the doped to the undoped cases. When doping takes place, antiferromagnetism can change to spin-glass magnetic behavior. On the other hand, when

there is little doping, the antiferromagnetic ordering is more stable, and the SWCNT leads the magnetic order of adsorbed dinuclear molecular magnets. However, in both cases, the nanotube diamagnetism vanishes, possibly due to the strong electron localization, caused by the adsorbed magnetic molecules that are able to disturb the molecular orbitals. Also, the magnetization is lower at high temperature as compared to pure SWCNT samples. Ideal superparamagnetism is unable to explain the hysteresis loops of the $Na_4[Cu_2(mpba)_2]\cdot 8H_2O$/SWCNT assembly. Two models, the mean field theory and a magneto-anisotropic nanoparticle model are used to fit the data in the low temperature range, both giving good fitting results.

Acknowledgments We thank Conselho Nacional de Desenvolvimento Científico e Tecnológico (CNPq), Fundação de Amparo à Pesquisa do Estado de Minas Gerais (FAPEMIG), Coordenação de Aperfeiçoamento de Pessoal de Nível Superior (CAPES), and Fundação de Amparo à Pesquisa do Estado de São Paulo (FAPESP) for financial support. We thank Miguel Julve for a private communication about the values of magnetization of the pure $Na_4[Cu_2(mpba)_2]\cdot 8H_2O$.

References

Almeida JRLd, Thouless DJ (1978) Stability study of the SK solution of a spin glass model. J Phys A 11:983

Bandyopadhyay M (2009) Thermodynamic properties of magneto-anisotropic nanoparticles. J Phy: Condens Matter 21:236003. doi:10.1088/0953-8984/21/23/236003

Beuneu F, l'Huillier C, Salvetat JP, Bonard JM, Forro L (1999) Modification of multiwall carbon nanotubes by electron irradiation: an ESR study. Phys Rev B 59(8):5945–5949. doi:10.1103/PhysRevB.59.5945

Bohn JE, Etchegoin PG, Ru ECL, Xiang R, Chiashi S, Maruyama S (2010) Estimating the raman cross sections of single carbon nanotubes. ACS Nano 4(6):3466–3470

Chichak KS, Star A, Altoé MVP, Stoddart JF (2005) Single-walled carbon nanotubes under the influence of dynamic coordination and supramolecular chemistry. Small 1(4): 452–461

Das S, Patra M, Majumdar S, Giri S (2009) Exchange bias effect at the irregular interfaces between Co and CoO nanostructures. J Alloy Compd 488:27–30

Du M, Jiang XJ, Zhao XJ, Cai H & Ribas J (2006) Novel metallosupramolecular networks constructed from Cu-II, Ni-II, and Cd-II with mixed ligands: crystal structures, fluorescence, and magnetism. Eu J Inorg Chem(6):1245–1254. doi:10.1002/ejic.200500822

Dul MC, Pardo E, Lescouezec R, Journaux Y, Ferrando-Soria J, Ruiz-Garcia R, Ruiz-Perez C (2010) Supramolecular coordination chemistry of aromatic polyoxalamide ligands: a metallosupramolecular approach toward functional magnetic materials [Review]. Coord Chem Rev 254(19–20):2281–2296. doi:10.1016/j.ccr.2010.03.003

Fainchtein R, Brown DM, Siegrist KM, Monica AH, Hwang ER, Milner SD, Davis CC (2012) Time-dependent near-blackbody thermal emission from pulsed laser irradiated vertically aligned carbon nanotube arrays. Phys Rev B 85(12):125432. doi:10.1103/PhysRevB.85.125432

Fernandez I, Ruiz R, Faus J, Julve M, Lloret F, Cano J, Munoz MC (2001) Ferromagnetic coupling through spin polarization in a dinuclear copper(II) metallacyclophane. Angew Chem-Intern Ed 40(16):3039–3042. doi:10.1002/1521-3757(20010817)113:16<3129:aid-ange3129>3.0.co;2-j

Ferrando-Soria J, Grancha T, Pasan J, Ruiz-Perez C, Canadillas-Delgado L, Journaux Y, Pardo E (2012) Solid-state aggregation of metallacyclophane-based Mn(II)Cu(II) one-dimensional Ladders. Inorg Chem 51(13):7019–7021. doi:10.1021/ic300953n

Feygenson M, Yiu Y, Kou A, Kim K-S, Aronson MC (2010) Controlling the exchange bias field in Co core/CoO shell nanoparticles. Phys Rev B 81:195445

Gonzalez JA, Andres JP, Toro JAD, Muniz P, Munoz T, Crisan O, Riveiro JM (2009) Co–CoO nanoparticles prepared by reactive gas-phase aggregation. J Nanopart Res 11: 2105–2111

Gupta V, Gupta BK, Kotnala RK, Narayanan TN, Grover V, Shah J, Agrawal V, Chand S, Shanker V (2011) Defect induced photoluminescence and ferromagnetic properties of bio-compatible SWCNT/Ni hybrid bundles. J Colloid Interface Sci 362(2):311–316. doi:10.1016/j.jcis.2011.06.074

Hamada N, Sawada S, Oshiyama A (1992) New one-dimensional conductors—graphitic microtubules. Phys Rev Lett 68(10):1579–1581. doi:10.1103/PhysRevLett.68.1579

Hua J, Lin WB (2004) Chiral metallacyclophanes: self-assembly, characterization, and application in asymmetric catalysis. Org Lett 6(6):861–864. doi:10.1021/ol036111v

Islam MF, Milkie DE, Torrens ON, Yodh AG, Kikkawa JM (2005) Magnetic heterogeneity and alignment of single wall carbon nanotubes. Phys Rev B 71:201401–201404

Kim YH, Choi J, Chang KJ, Tomanek D (2003) Defective fullerenes and nanotubes as molecular magnets: an ab initio study. Phys Rev B 68(12):125420. doi:10.1103/PhysRevB.68.125420

Li RK, Greaves C (2004) One-dimensional ferromagnetism of gaudefroyite $Ca_4(MnO)_3(BO_3)_3CO_3$. Phys Rev B 70(13):132411. doi:10.1103/PhysRevB.70.132411

Likodimos V, Glenis S, Guskos N, Lin CL (2007) Antiferromagnetic behavior in single-wall carbon nanotubes. Phys Rev B 76(7):075420. doi:10.1103/PhysRevB.76.075420

Lin R, Yip JHK, Zhang K, Koh LL, Wong KY, Ho KP (2004) Self-assembly and molecular recognition of a luminescent gold rectangle [Review]. J Am Chem Soc 126(48):15852–15869. doi:101021/ja0456508

Lu J, J-x Yang, Wang J, Lim A, Wang S, Loh KP (2009) One-pot synthesis of fluorescent carbon nanoribbons, nanoparticles, and graphene by the exfoliation of graphite in ionic liquids. ACS Nano 3(8):2367–2375

Mintmire JW, Dunlap BI, White CT (1992) Are fullerene tubules metallic? Phys Rev Lett 68(5):631–634. doi:10.1103/PhysRevLett.68.631

Pardo E, Cangussu D, Lescouezec R, Journaux Y, Pasan J, Delgado FS, Lloret F (2009) Molecular-programmed self-assembly of homo- and heterometallic tetranuclear

coordination compounds: synthesis, crystal structures, and magnetic properties of rack-type (Cu_2M_2II)−M−II complexes (M = Cu and Ni) with tetranucleating phenylenedioxamato bridging ligands [Article]. Inorg Chem 48(11):4661–4673. doi:10.1021/ic900055d

Park JS, Sasaki K, Saito R, Izumida W, Kalbac M, Farhat H, Dresselhaus MS (2009) Phys Rev B 80:081402(R)

Pereira CLM, Pedroso EF, Stumpf HO, Novak MA, Ricard L, Ruiz-Garcia R, Journaux Y (2004) A (CuCoII)−Co−II metallacyclophane-based metamagnet with a corrugated brick-wall sheet architecture. Ang Chem -Int Ed 43(8):955–958. doi:10.1002/anie.200352604

Qian Z, Wang C, Feng H, Chen C, Zhou J, Chen J (2011) Well dispersed single-walled carbon nanotubes with strong visible fluorescence in water for metal ions sensing. Chem Commun 47:7167–7169

Sáfar GAM, CarvalhoDa-Silva D, Idemori YM, Ribeiro HB, Fantini C, Plentz FO, Rebouças JS (2010) Measuring the electronic properties of single-walled carbon nanotubes with adsorbed porphyrins using optical transitions. J Porph Phthalocyanines 14:885–890

Sáfar GAM, Barros WP, Idemori YM, CarvalhoDa-Silva D, Mendes JBS, Sinnecker EHCP, Stumpf HO (2012) Multiple magnetic characteristics in pure and Mn porphyrin-doped single-walled carbon nanotubes. J Nanopart Res 14(6):912. doi:10.1007/s11051-012-0912-7

Saito R, Fujita M, Dresselhaus G, Dresselhaus MS (1992) Electronic-structure of chiral graphene tubules. Appl Phys Lett 60(18):2204–2206. doi:10.1063/1.107080

Shina NC, Leea Y-H, Shina YH, Kimb J, Lee Y-W (2010) Synthesis of cobalt nanoparticles in supercritical methanol. Mater Chem Phys 124:140–144

Steuerman DW, Star A, Narizzano R, Choi H, Ries RS, Nicolini C, Heath JR (2002) Interactions between conjugated polymers and single-walled carbon nanotubes. J Phys Chem B 106:3124–3130

Tan PH, Rozhin AG, Hasan T, Hu P, Scardaci V, Milne WI, Ferrari AC (2007) Photoluminescence spectroscopy of carbon nanotube bundles: evidence for exciton energy transfer. Phys Rev Lett 99:137402

Wang X, Cao L, Bunker CE, Meziani MJ, Lu F, Guliants EA, Sun Y-P (2010) Fluorescence decoration of defects in carbon nanotubes. J Phys Chem C 114:20941–20946